Entanglement of electrons and lattice in a Luttinger system

Gergő Roósz[1,2] and Carsten Timm[1,3,*]

[1]*Institute of Theoretical Physics, Technische Universität Dresden, 01062 Dresden, Germany*

[2]*Institute for Solid State Physics and Optics, Wigner Research Centre for Physics, P.O. Box 49, 1525 Budapest, Hungary*

[3]*Würzburg-Dresden Cluster of Excellence ct.qmat, Technische Universität Dresden, 01062 Dresden, Germany*

(Received 5 February 2021; revised 15 June 2021; accepted 21 June 2021; published 2 July 2021)

The coupling between electronic and lattice degrees of freedom lies at the core of many important properties of solids. Nevertheless, surprisingly little is known about the entanglement between these degrees of freedom. Here, we calculate the entanglement entropy at zero temperature as well as the mutual information and the logarithmic entanglement negativity at finite temperatures between the electrons and the lattice for a one-dimensional chain. The electrons are described within Luttinger-liquid theory. Our results show that the entanglement entropy diverges when one approaches the limit of stability, the so-called Wentzel-Bardeen singularity. We find that the mutual information and the logarithmic entanglement negativity decrease with temperature. The mutual information reaches a finite value in the infinite-temperature limit, which is a consequence of the infinite linear electron spectrum of Luttinger theory. The logarithmic entanglement negativity becomes exactly zero above a certain temperature; that is, the lattice and the electrons become nonentangled above this temperature. If the electron-electron interaction is unscreened or weakly screened, this characteristic temperature diverges with the system size. However, if the interaction is strongly screened, the characteristic temperature is finite and independent of size, indicating a phase transition in the thermodynamic limit.

DOI: 10.1103/PhysRevB.104.035405

I. INTRODUCTION

In the study of solids, one often starts with the adiabatic (and approximate) decoupling of the electronic and lattice degrees of freedom. However, these subsystems are not independent, and their coupling causes many interesting phenomena in condensed matter systems, for example, BCS-type superconductivity [1–6], the Peierls instability [7–9], and charge-density-wave formation [10–12]. The description of the coupled electron-phonon system is a nontrivial problem. Sophisticated approximations, such as diagrammatic perturbation theory [13,14], Monte Carlo simulations [15–17], and the tensor-network approach [18], have been developed.

Advances in quantum information theory in the last two decades have made it possible to quantify correlations and entanglement between subsystems without depending on concrete correlation functions and observables [19,20]. This has led to a better understanding of thermalization [21] and simulability [22] of quantum systems. In this context, the entanglement entropy between the electron and the protons in the H_2^+ molecular ion has been calculated [23], but we are not aware of similar studies for extended systems. This paper describes a step in this direction.

In order to obtain precise knowledge about the whole spectrum and the wave functions of all excited states, we use an integrable model, which, on the other hand, should have the power to describe strongly interacting systems. Such a model exists for one dimension, namely, the Luttinger liquid coupled to acoustic phonons, which was introduced by Wentzel [24] and Bardeen [25]. This model is best known for the Wentzel-Bardeen singularity: For sufficiently strong electron-phonon coupling, the Hamiltonian becomes unbounded from below. Early work on the Wentzel-Bardeen singularity was motivated by its suspected analogy with superconductivity in higher-dimensional systems [24–26], which, however, was ultimately not productive.

Similar models can be used to describe the electron-phonon coupling in carbon nanotubes [27–31], and there has been speculation that the Wentzel-Bardeen singularity could be realized in these systems [30]. Notably, in certain nanotube systems the electron-phonon interaction is tunable by adding quantum dots to the nanotube [32]. In Refs. [29–31], models with multiple phonon branches and multiple electronic bands are employed, and the phonons are described by a continuum model. For the sake of a transparent and compact treatment, we here consider one electronic band and one acoustic phonon branch. The inclusion of multiple electronic bands and several phonon branches, as required for a realistic description of specific nanotubes, is technically straightforward. Moreover, we start from a discrete lattice, which is more natural and avoids the necessity of a cutoff.

We will characterize the correlations and entanglement using the following measures: At zero temperature, the entanglement entropy will be used [33,34]. The system is in its ground state $|\mathrm{GS}\rangle$, and its density matrix is the projector $\rho = |\mathrm{GS}\rangle\langle\mathrm{GS}|$. One divides the system into two complementary parts A and B, which in our case are the electrons and the lattice. The reduced density matrices of the two subsystems are

$$\rho_A = \mathrm{Tr}_B \rho, \quad \rho_B = \mathrm{Tr}_A \rho, \tag{1}$$

*carsten.timm@tu-dresden.de

where Tr_A and Tr_B denote the partial trace over subsystem A and B, respectively. The entanglement entropy is defined as the von Neumann entropy of the reduced density matrices,

$$S = -\mathrm{Tr}_B \rho_B \ln \rho_B = -\mathrm{Tr}_A \rho_A \ln \rho_A. \tag{2}$$

At nonzero temperatures, the total (quantum and classical) correlations are characterized by the mutual information [35]. To define the mutual information, one first introduces the entropies of the reduced density matrices,

$$S_A = -\mathrm{Tr}_A \rho_A \ln \rho_A, \tag{3}$$

$$S_B = -\mathrm{Tr}_B \rho_B \ln \rho_B. \tag{4}$$

These two entropies are generally different, $S_A \neq S_B$. The mutual information is defined as

$$I(A:B) = S_A + S_B - S_{A\cup B}, \tag{5}$$

where $S_{A\cup B} = -\mathrm{Tr}\rho \ln \rho$ is the entropy of the whole system.

In order to characterize the *quantum* correlations at nonzero temperatures, we use the entanglement negativity [36,37]. Its definition relies on the concept of the partial transpose ρ^{T_A} of the density matrix, which is defined in terms of matrix elements with respect to the product basis of subsystems A and B as

$$\langle a_i, b_j|\rho^{T_A}|a_n, b_m\rangle = \langle a_n, b_j|\rho|a_i, b_m\rangle. \tag{6}$$

The partial transpose is unitarily equivalent to a time reversal in subsystem A since the time reversal of observables is represented by a product of a unitary transformation and a transposition. It turns out that classical states, i.e., states without entanglement, have no knowledge about the common time direction. The partial transpose of the density matrix is then also a valid density matrix with all eigenvalues positive [36,37]. On the other hand, if the state is entangled, negative eigenvalues may occur in the partial transpose. The sum of these negative eigenvalues is a so-called entanglement monotone; that is, it does not decrease in absolute value under local operations and classical communication (LOCC) [38].

The negativity is defined as the sum of the absolute values of the negative eigenvalues of the partial transpose,

$$\mathcal{N} = \sum_{\lambda_i<0} |\lambda_i| = \frac{||\rho^{T_A}||_1 - 1}{2}, \tag{7}$$

where the λ_i are the eigenvalues of ρ^{T_A} and $||\bullet||_1$ is the trace norm, which is defined as the sum of the absolute values of the eigenvalues. The logarithmic negativity is then defined as

$$\mathcal{E}_\mathcal{N} = \ln(2\mathcal{N}+1) = \ln||\rho^{T_A}||_1. \tag{8}$$

The remainder of this paper is organized as follows: In Sec. II, we define our model and present its solution. The values of the relevant correlation functions are also given. In Sec. III, we then express the entanglement measures in terms of integrals, which are evaluated numerically in Sec. IV. (The continuum limit is briefly discussed in Appendix.) Finally, we summarize and discuss our results in Sec. V.

II. MODEL

The lattice is modeled as a harmonic-oscillator chain with periodic boundary conditions, which is coupled to a one-dimensional Luttinger liquid [24–26]. If one turns off the electron-electron interaction, this model is equivalent to the original Wentzel-Bardeen model studied in Refs. [24–26]. We note that this problem can be treated by integrating out the phonons, which gives an effective electronic model [39]. Here, we do not follow this approach since we need to keep the phonons in order to characterize the electron-phonon entanglement and correlations. After bosonization, we use methods derived for oscillator systems [40–42] to characterize the entanglement.

The system is defined by the Hamiltonian

$$\begin{aligned} H = &-\sum_{\sigma=\pm1/2}\int_0^L \frac{dx}{2\pi}\, v_f [{}^*_*\Psi^\dagger_{\sigma,L}(x)\, i\partial_x \Psi_{\sigma,L}(x){}^*_* \\ &\qquad - {}^*_*\Psi^\dagger_{\sigma,R}(x)\, i\partial_x \Psi_{\sigma,R}(x){}^*_*] \\ &+ \sum_{j=1}^N \frac{p_j^2}{2} + \frac{1}{2}\kappa(q_j - q_{j+1})^2 \\ &+ \frac{1}{\sqrt{L}}\sum_{j=1}^L q_j \int_0^L dx\, [\hat{n}_L(x) + \hat{n}_R(x)] g(|x - ja_0|_L) \\ &+ \frac{4}{L}\int_0^L\int_0^L dx\, dy\, (\hat{n}_L(x), \hat{n}_R(y)) \\ &\quad \times \begin{pmatrix} h(x-y) & \frac{1}{2}f(x-y) \\ \frac{1}{2}f(x-y) & h(x-y) \end{pmatrix} \begin{pmatrix} \hat{n}_L(x) \\ \hat{n}_R(y) \end{pmatrix}, \end{aligned} \tag{9}$$

where L is the length of the system and the symbol ${}^*_*\bullet{}^*_*$ denotes normal ordering. The lattice constant is $a_0 = L/N$, where N is the number of the oscillators. The equilibrium positions of the atoms are $x_j = j$. The field operators $\Psi^\dagger_{\sigma,L}(x)$, $\Psi^\dagger_{\sigma,R}(x)$ create an electron with spin $\sigma = \pm 1/2$ at site x, where L and R stand for the left-going and right-going electrons, respectively. The first two terms in Eq. (9) denote the kinetic energy of the electrons, where the factor 2π stems from the normalization of the fields [43]. The third line describes the lattice system, where q_j and p_j are the Hermitian canonical position and momentum operators of atom j. The fourth line corresponds to the electron-phonon coupling. The local electron densities are $\hat{n}_L(x) = \sum_\sigma \Psi^\dagger_{\sigma,L}(x)\Psi_{\sigma,L}(x)$ and $\hat{n}_R(x) = \sum_\sigma \Psi^\dagger_{\sigma,R}(x)\Psi_{\sigma,R}(x)$. The displacements of the oscillators couple to the electron density in a nonlocal manner described by the function $g(|x-j|_L)$, where $|x-j|_L$ is the shortest distance between x and j, taking periodic boundary conditions into account.

In Refs. [24–26], it was supposed that the Fourier transform g_k of $g(\Delta x)$ is linear for small k, i.e., $g_k \sim k$. This may go back to old work by Bloch [44], which indeed predicts linear electron-phonon coupling. It has become clear, though, that the picture of a homogeneous positive background used in the derivation of the Bloch formula is too crude [45] and that the electron-phonon coupling is generally not linear in the wave number k. In a number of real one-dimensional systems, the

electron-phonon coupling is found to be $g_k \sim \sqrt{k}$ [29,45]. We will discuss both forms of electron-phonon coupling below.

The last two lines in Eq. (9) describe the electron-electron interaction, which is assumed to be spin independent. The interaction between electrons moving in the same direction (opposite directions) is described by the function $h(x-y)$ [$f(x-y)$]. Since the function $h(x-y)$ describes processes with small momentum transfer, whereas $f(x-y)$ corresponds to processes with large momentum transfer on the order of $2k_F$, $h(x-y)$ is expected to be larger than $f(x-y)$. Depending on screening, the Fourier transform h_k of $h(x-y)$ may be singular at $k=0$. We will discuss singularities of the power-law form $h_k \sim 1/k^\alpha$ below. We suppose that the function $f(x-y)$ and its Fourier transform are regular. The factor of 4 is included in Eq. (9) for later convenience.

The electron operators in momentum space are

$$c_{k,\sigma,\nu} = \sqrt{\frac{2\pi}{L}} \int_{-L/2}^{L/2} dx\, e^{ikx}\, \Psi_{\sigma,\nu}(x), \tag{10}$$

$$c^\dagger_{k,\sigma,\nu} = \sqrt{\frac{2\pi}{L}} \int_{-L/2}^{L/2} dx\, e^{-ikx}\, \Psi^\dagger_{\sigma,\nu}(x), \tag{11}$$

where $k = (2\pi/L)\,n$ with $n \in \mathbb{Z}$. The factor $\sqrt{2\pi}$ results from the normalization of the field [43]. In the next step, we construct the bosonic operators

$$b_{\sigma,\nu,q} = \frac{1}{\sqrt{n_k}} \sum_{k=-\infty}^{\infty} c^\dagger_{\sigma,\nu,k+q} c_{\sigma,\nu,k}, \tag{12}$$

$$b^\dagger_{\sigma,\nu,q} = \frac{1}{\sqrt{n_k}} \sum_{k=-\infty}^{\infty} c^\dagger_{\sigma,\nu,k} c_{\sigma,\nu,k+q}. \tag{13}$$

Using these operators, we define Hermitian position and momentum operators for the electronic degrees of freedom as

$$q_{k,\eta,1} = \sum_{\sigma=\pm1/2} \frac{(-1)^{\eta(\sigma+1/2)}}{\sqrt{8}\sqrt{\Omega_k}} \times (b^\dagger_{k,\sigma} + b_{k,\sigma} + b^\dagger_{-k,\sigma} + b_{-k,\sigma}), \tag{14}$$

$$q_{k,\eta,2} = \sum_{\sigma=\pm1/2} \frac{-i(-1)^{\eta(\sigma+1/2)}}{\sqrt{8}\sqrt{\Omega_k}} \times (b^\dagger_{k,\sigma} - b_{k,\sigma} - b^\dagger_{-k,\sigma} + b_{-k,\sigma}), \tag{15}$$

$$p_{k,\eta,1} = \sum_{\sigma=\pm1/2} \frac{i\sqrt{\Omega_k}(-1)^{\eta(\sigma+1/2)}}{\sqrt{8}} \times (b^\dagger_{k,\sigma} - b_{k,\sigma} + b^\dagger_{-k,\sigma} - b_{-k,\sigma}), \tag{16}$$

$$p_{k,\eta,2} = \sum_{\sigma=\pm1/2} \frac{\sqrt{\Omega_k}(-1)^{\eta(\sigma+1/2)}}{\sqrt{8}} \times (b^\dagger_{k,\sigma} + b_{k,\sigma} - b^\dagger_{-k,\sigma} - b_{-k,\sigma}), \tag{17}$$

where $k \geqslant 0$ and $\eta = 0$ ($\eta = 1$) corresponds to the charge (spin) modes. These operators satisfy the canonical commutation relations $[q_{k,\eta,j}, q_{q,\eta,i}] = [p_{k,\eta,j}, p_{q,\eta,i}] = 0$ and $[q_{k,\eta,j}, p_{q,\eta',i}] = i\delta_{q,k}\delta_{\eta,\eta'}\delta_{i,j}$. The frequency Ω_k is defined as $\Omega_k = v_f k + (5/4\pi)\,h_k k$.

Turning to the lattice degrees of freedom, we introduce the Hermitian sine and cosine modes

$$Q_{S,k} = \sqrt{\frac{2}{L}} \sum_{n=1}^{L} \sin(kn)\, q_n, \tag{18}$$

$$P_{S,k} = \sqrt{\frac{2}{L}} \sum_{n=1}^{L} \sin(kn)\, p_n, \tag{19}$$

$$Q_{C,k} = \sqrt{\frac{2}{L}} \sum_{n=1}^{L} \cos(kn)\, q_n, \tag{20}$$

$$P_{C,k} = \sqrt{\frac{2}{L}} \sum_{n=1}^{L} \cos(kn)\, p_n. \tag{21}$$

The inverse transformations read as

$$q_n = \sqrt{\frac{2}{L}} \sum_{k} [\cos(kn)\, Q_{C,k} + \sin(kn)\, Q_{S,k}], \tag{22}$$

$$p_n = \sqrt{\frac{2}{L}} \sum_{k} [\cos(kn)\, P_{C,k} + \sin(kn)\, P_{S,k}]. \tag{23}$$

We finally obtain the Hamiltonian in oscillator form,

$$\begin{aligned} H = {} & \sum_{k=0}^{\infty} \sum_{\eta=0,1} \left(\Omega_k + \frac{1}{2}\, p^2_{k,\eta,1} + \frac{1}{2}\, \Omega_k^2 q^2_{k,\eta,1} \right. \\ & \left. + \frac{1}{2}\, p^2_{k,\eta,2} + \frac{1}{2}\, \Omega_k^2 q^2_{k,\eta,2} \right) \\ & + \sum_{k=0}^{\pi} \frac{P^2_{S,k}}{2m} + \frac{1}{2}\, \omega_k m Q^2_{S,k} + \frac{P^2_{C,k}}{2m} + \frac{1}{2}\, \omega_k m Q^2_{C,k} \\ & + \sum_{k=0}^{\pi} g_k \sqrt{2 n_k \Omega_k} (Q_{C,k} q_{k,0,1} + Q_{S,k} q_{k,0,2}) \\ & + \sum_{k=0}^{\pi} \frac{5}{4\pi}\, k f_k \left(\frac{1}{2}\, \Omega_k q^2_{k,0,1} - \frac{1}{2\Omega_k}\, p^2_{k,0,1} \right. \\ & \left. + \frac{1}{2}\, \Omega_k q^2_{k,0,2} - \frac{1}{2\Omega_k}\, p^2_{k,0,2} \right), \end{aligned} \tag{24}$$

where the frequency of the phonon modes is $\omega_k = 2\sqrt{\kappa}\,|\sin k/2|$.

A. Diagonalization

The Hamiltonian in Eq. (24) can be diagonalized by a canonical transformation. The charge modes with $|k| > \pi$ do not couple to the lattice and are thus left unchanged during the diagonalization. Similarly, the spin modes, represented by $q_{k,1,1}$, $q_{k,1,2}$, $p_{k,1,1}$, $p_{k,1,2}$, do not couple to the lattice for any k and are also unchanged.

The diagonalized Hamiltonian is

$$\begin{aligned} H = {} & \sum_{k=0}^{\infty} \left(\Omega_k + \frac{1}{2}\, p^2_{k,1,1} + \frac{1}{2}\, \Omega_k^2 q^2_{k,1,1} \right. \\ & \left. + \frac{1}{2}\, p^2_{k,1,2} + \frac{1}{2}\, \Omega_k^2 q^2_{k,1,2} \right) \end{aligned}$$

$$+\sum_{k=\pi}^{\infty}\Big(\frac{1}{2}\,p_{k,0,1}^2+\frac{1}{2}\,\Omega_k^2 q_{k,0,1}^2+\frac{1}{2}\,p_{k,0,2}^2+\frac{1}{2}\,\Omega_k^2 q_{k,0,2}^2\Big)+\sum_{k=0}^{\pi}\Big(\frac{P_{1,+,k}^2}{2}+\frac{1}{2}\,\lambda_{+,k}Q_{1,+,k}^2+\frac{P_{1,-,k}^2}{2}+\frac{1}{2}\,\lambda_{-,k}Q_{1,+,k}^2+\frac{P_{2,+,k}^2}{2}+\frac{1}{2}\,\lambda_{+,k}Q_{2,-,k}^2+\frac{P_{2,-,k}^2}{2}+\frac{1}{2}\,\lambda_{-,k}Q_{2,+,k}^2\Big),\tag{25}$$

with

$$\lambda_{k,\pm}=\frac{1}{2}\Big[\omega_k^2+\Big(\Omega_k^2+\frac{5}{4\pi}kf_k\Big)\alpha_k^2\Big]\pm\frac{1}{2}\sqrt{\Big[\omega_k^2-\Big(\Omega_k^2+\frac{5}{4\pi}kf_k\Big)\alpha_k^2\Big]^2+\frac{4}{\pi}g_k^2k\Omega_k\alpha_k^2},\tag{26}$$

where

$$\alpha_k=\sqrt{1-\frac{f_k}{\frac{4\pi}{5}v_F+h_k}}.\tag{27}$$

The nontrivial eigenfrequencies of the diagonalized Hamiltonian are given by $\sqrt{\lambda_{k,\pm}}$. The radicand $\lambda_{k,\pm}$ can be negative if the Hamiltonian is not bounded from below and the system is unstable. This is the Wentzel-Bardeen singularity [24,25]. The stability criterion reads as [26]

$$\omega_k^2\Big[v_f+\frac{5}{4\pi}(f_k+h_k)\Big]>\frac{g_k^2}{\pi}.\tag{28}$$

The coupled electron-lattice eigenmodes appearing in the diagonalized Hamiltonian in Eq. (25) are given by

$$P_{1,\pm,k}=\alpha_k(A_{\pm,k}P_{C,k}+B_{\pm,k}p_{k,0,1}),\tag{29}$$

$$Q_{1,\pm,k}=\frac{A_{\pm,k}Q_{C,k}+B_{\pm,k}q_{k,0,1}}{\alpha_k},\tag{30}$$

$$P_{2,\pm,k}=\alpha_k(A_{\pm,k}P_{S,k}+B_{\pm,k}p_{k,0,2}),\tag{31}$$

$$Q_{2,\pm,k}=\frac{A_{\pm,k}Q_{S,k}+B_{\pm,k}q_{k,0,2}}{\alpha_k},\tag{32}$$

where

$$A_{\pm,k}=-\frac{1}{\sqrt{N_k}}\,g_k\sqrt{\frac{k\Omega_k}{4\pi}}\sqrt{1-\frac{\frac{5}{4\pi}f_k}{v_F+\frac{5}{4\pi}h_k}},\tag{33}$$

$$B_{\pm,k}=\frac{1}{\sqrt{N_k}}\left(\omega_k^2-\lambda_{\pm}\right),\tag{34}$$

$$N_k=\left(\omega_k^2-\lambda_{\pm}\right)^2+g_k^2\frac{k\Omega_k}{4\pi}\sqrt{1-\frac{\frac{5}{4\pi}f_k}{v_F+\frac{5}{4\pi}h_k}}.\tag{35}$$

Finally, these oscillator eigenmodes can be expressed in terms of the bosonic operators

$$a_{i,\pm,k}=\frac{\lambda_{k,\pm}^{1/4}}{\sqrt{2}}\left(Q_{i,\pm,k}+i\,\frac{1}{\lambda_{k,\pm}^{1/4}}\,P_{i,\pm,k}\right),\tag{36}$$

$$a_{i,\pm,k}^{\dagger}=\frac{\lambda_{k,\pm}^{1/4}}{\sqrt{2}}\left(Q_{i,\pm,k}-i\,\frac{1}{\lambda_{k,\pm}^{1/4}}\,P_{i,\pm,k}\right).\tag{37}$$

With the solution in hand, we can calculate the pair correlation functions.

B. Correlation functions

The entanglement measures can be calculated from pair correlation functions. The correlation functions of the lattice sine and cosine modes read as

$$\langle Q_{S,k}^2\rangle=\langle Q_{C,k}^2\rangle=\frac{1}{\alpha_k^2}\left[\frac{A_{k,+}^2}{2\lambda_{k,+}^{1/2}}\left(\frac{2}{e^{\beta\lambda_{k,+}^{1/2}}-1}+1\right)+\frac{A_{k,-}^2}{2\lambda_{k,-}^{1/2}}\left(\frac{2}{e^{\beta\lambda_{k,-}^{1/2}}-1}+1\right)\right],\tag{38}$$

$$\langle P_{S,k}^2\rangle=\langle P_{C,k}^2\rangle=\alpha_k^2\left[\frac{A_{k,+}^2\lambda_{k,+}^{1/2}}{2}\left(\frac{2}{e^{\beta\lambda_{k,+}^{1/2}}-1}+1\right)+\frac{A_{k,-}^2\lambda_{k,-}^{1/2}}{2}\left(\frac{2}{e^{\beta\lambda_{k,-}^{1/2}}-1}+1\right)\right].\tag{39}$$

The correlation functions of the coupled electronic charge modes are

$$\langle q_{k,0,1}^2\rangle=\langle q_{k,0,2}^2\rangle=\frac{1}{\alpha_k^2}\left[\frac{B_{k,+}^2}{2\lambda_{k,+}^{1/2}}\left(\frac{2}{e^{\beta\lambda_{k,+}^{1/2}}-1}+1\right)+\frac{B_{k,-}^2}{2\lambda_{k,-}^{1/2}}\left(\frac{2}{e^{\beta\lambda_{k,-}^{1/2}}-1}+1\right)\right],\tag{40}$$

$$\langle p_{k,0,1}^2\rangle=\langle p_{k,0,2}^2\rangle=\alpha_k^2\left[\frac{B_{k,+}^2\lambda_{k,+}^{1/4}}{2}\left(\frac{2}{e^{\beta\lambda_{k,+}^{1/4}}-1}+1\right)+\frac{B_{k,-}^2\lambda_{k,-}^{1/4}}{2}\left(\frac{2}{e^{\beta\lambda_{k,-}^{1/4}}-1}+1\right)\right].\tag{41}$$

Finally, the correlation functions connecting the lattice and electronic charge modes read as

$$\langle Q_{S,k}\,q_{k,0,2}\rangle=\langle Q_{C,k}\,q_{k,0,1}\rangle=\frac{A_{+,k}B_{+,k}}{2\lambda_{k,+}^{1/2}}\left(\frac{2}{e^{\beta\lambda_{k,+}^{1/2}}-1}+1\right)+\frac{A_{-,k}B_{-,k}}{2\lambda_{k,-}^{1/2}}\left(\frac{2}{e^{\beta\lambda_{k,-}^{1/2}}-1}+1\right),\tag{42}$$

$$\langle P_{S,k}\,p_{k,0,2}\rangle=\langle P_{C,k}\,p_{k,0,1}\rangle=\frac{A_{+,k}B_{+,k}\lambda_{k,+}^{1/2}}{2}\left(\frac{2}{e^{\beta\lambda_{k,+}^{1/2}}-1}+1\right)+\frac{A_{-,k}B_{-,k}\lambda_{k,-}^{1/2}}{2}\left(\frac{2}{e^{\beta\lambda_{k,-}^{1/2}}-1}+1\right).\tag{43}$$

The correlation functions connecting the electronic spin modes to the charge or lattice modes are zero, as are the correlation functions connecting the electronic charge modes with $|k| > \pi$ to the lattice.

III. ENTANGLEMENT AND CORRELATION MEASURES

In this section we describe the calculation of the measures of entanglement and correlations. Most of them are expressed by sums of analytical terms. The starting point is the equilibrium density matrix of the system, which is a bosonic Gaussian operator.

A. Entanglement entropy

At zero temperature, we consider the entanglement entropy between the electron and lattice degrees of freedom. The entanglement entropy is calculated using the correlation-function method [46], which has been used to investigate momentum-space entanglement in a Luttinger liquid [47] and entanglement entropy in multicomponent Luttinger systems [48,49]. We first define the correlation matrices of the lattice,

$$Q_{i,j} = \langle \mathrm{GS}|q_i q_j|\mathrm{GS}\rangle, \quad P_{i,j} = \langle \mathrm{GS}|p_i p_j|\mathrm{GS}\rangle. \tag{44}$$

Let the spectrum of the matrix $C = QP$ be $\nu_1 \ldots, \nu_L$. The entanglement entropy is then

$$S = \sum_{j=1}^{L} \left[\left(\sqrt{\nu_j} + \frac{1}{2}\right) \ln\left(\sqrt{\nu_j} + \frac{1}{2}\right) - \left(\sqrt{\nu_j} - \frac{1}{2}\right) \ln\left(\sqrt{\nu_j} - \frac{1}{2}\right) \right]. \tag{45}$$

Introducing the function $s(x) = (\sqrt{x} + 1/2)\ln(\sqrt{x} + 1/2) - (\sqrt{x} - 1/2)\ln(\sqrt{x} - 1/2)$, we can rewrite this as

$$S = \mathrm{Tr}\, s(C), \tag{46}$$

where the trace has to be computed on the L-dimensional space C acts on. Performing the trace with respect to the common eigenbasis of Q and P, i.e., the sine-cosine basis, we obtain a simple equation for the entanglement entropy:

$$S = \sum_{k>0}^{\pi} \left[s\left(\langle Q_{S,k}^2\rangle \langle P_{S,k}^2\rangle\right) + s\left(\langle Q_{C,k}^2\rangle \langle P_{C,k}^2\rangle\right)\right]. \tag{47}$$

This sum is easily calculated numerically. The results are shown in Sec. IV. In the thermodynamic limit, $L \gg 1$, the sum is replaced by the integral

$$S = \frac{L}{2\pi} \int_0^{\pi} dk \left[s\left(\langle Q_{S,k}^2\rangle \langle P_{S,k}^2\rangle\right) + s\left(\langle Q_{C,k}^2\rangle \langle P_{C,k}^2\rangle\right)\right]. \tag{48}$$

Since the integral is finite, the entropy scales as $S \sim L$.

The reduced density matrix ρ_{ph} of the phonons can be written in a simple form using the Hermitian canonical operators of the sine and cosine modes. For any temperature including $T = 0$, it reads as

$$\rho_{\mathrm{ph}} = \frac{1}{Z} \prod_{k>0}^{\pi} e^{-\beta_k^{\mathrm{eff}}\left(\frac{1}{2}P_{C,k}^2 + \frac{1}{2}\omega_k^{\mathrm{eff}} Q_{C,k}^2\right)} \times e^{-\beta_k^{\mathrm{eff}}\left(\frac{1}{2}P_{S,k}^2 + \frac{1}{2}\omega_k^{\mathrm{eff}} Q_{S,k}^2\right)}, \tag{49}$$

where

$$\beta_k^{\mathrm{eff}} = \frac{\sigma_k^Q}{\sigma_k^P} \ln \frac{\sigma_k^Q \sigma_k^P + 1/2}{\sigma_k^Q \sigma_k^P - 1/2}, \tag{50}$$

$$\omega_k^{\mathrm{eff}} = \frac{\sigma_k^P}{\sigma_k^Q}, \tag{51}$$

and

$$\sigma_k^Q = \sqrt{\langle Q_{C,k}^2\rangle} = \sqrt{\langle Q_{S,k}^2\rangle}, \tag{52}$$

$$\sigma_k^P = \sqrt{\langle P_{C,k}^2\rangle} = \sqrt{\langle P_{S,k}^2\rangle} \tag{53}$$

are the variances of the position and momentum operators, respectively.

B. Mutual information

At nonzero temperatures, we calculate the mutual information between the electron and lattice degrees of freedom, which characterizes the total correlation between the two subsystems. The mutual information is defined as

$$I = S_{\mathrm{ph}} + S_{\mathrm{el}} - S_{\mathrm{ph}\cup\mathrm{el}}. \tag{54}$$

The density matrix of the whole system can be written as

$$\rho_{\mathrm{ph}\cup\mathrm{el}} = \rho_1 \otimes \rho_s \otimes \rho_c, \tag{55}$$

with

$$\rho_1 = \frac{1}{Z_1} \prod_{|q|>\pi,\sigma}^{\infty} e^{-\beta|q|v_f b_{q,\sigma}^\dagger b_{q,\sigma}}, \tag{56}$$

$$\rho_s = \frac{1}{Z_s} \prod_{|q|<\pi} e^{-\beta|q|v_f b_{S,q,\sigma}^\dagger b_{S,q,\sigma}}, \tag{57}$$

$$\rho_c = \frac{1}{Z_c} \prod_{k>0,\pm,j=1,2}^{\pi} e^{-\beta\lambda_{k,\pm}^{1/2} a_{k,\pm,j}^\dagger a_{k,\pm,j}}. \tag{58}$$

Here, ρ_1 describes the uncoupled short-wavelength excitations, which are present because the fermions are described by a continuum model, ρ_s describes the uncoupled electronic spin modes, and ρ_c describes the coupled electron-phonon modes. Z_1, Z_s, and Z_c are the corresponding partition functions, which simply ensure that the density matrices have unit trace.

The terms referring to the uncoupled electronic modes cancel each other in Eq. (54) so that the mutual information is determined only by the density matrix of the coupled modes,

$$I = S(\mathrm{Tr}_{\mathrm{ph}}\rho_c) + S(\mathrm{Tr}_{\mathrm{el}}\rho_c) - S(\rho_c). \tag{59}$$

The three terms are given by

$$S(\mathrm{Tr}_{\mathrm{ph}}\rho_c) = \sum_{k>0}^{\pi} \left[s\left(\langle Q_{S,k}^2\rangle \langle P_{S,k}^2\rangle\right) + s\left(\langle Q_{C,k}^2\rangle \langle P_{C,k}^2\rangle\right)\right], \tag{60}$$

$$S(\mathrm{Tr}_{\mathrm{el}}\rho_c) = \sum_{k>0}^{\pi} \left[s\left(\langle q_{k,0,1}^2\rangle \langle p_{k,0,1}^2\rangle\right) + s\left(\langle q_{k,0,2}^2\rangle \langle p_{k,0,2}^2\rangle\right)\right], \tag{61}$$

$$S(\rho_c) = 2\sum_{k>0,\pm}^{\pi}\left[\frac{\sqrt{\lambda}_{k,\pm}}{\exp(\beta\sqrt{\lambda}_{k,\pm})-1} - \ln(1-\exp(-\beta\sqrt{\lambda}_{k,\pm}))\right]. \quad (62)$$

These sums are easily calculated numerically. The results are presented in Sec. IV.

C. Entanglement negativity

The logarithmic negativity has been defined in Eq. (8). The partial transpose can be considered for any factor space of the Hilbert space. Here, we would like to characterize the electron-phonon entanglement; therefore we consider the partial transpose for the phonon sector. The density matrix of the system is the tensor product

$$\rho_{\mathrm{ph}\cup\mathrm{el}} = \rho_1 \otimes \rho_s \otimes \rho_c. \quad (63)$$

The partial transpose only affects the third term. We write the result as

$$\rho^{\Gamma}_{\mathrm{ph}\cup\mathrm{el}} = \rho_1 \otimes \rho_s \otimes \rho_c^{T_{\mathrm{ph}}}. \quad (64)$$

We introduce the following notation for the eigenvectors and eigenvalues of the operators ρ_1, ρ_s, and $\rho_c^{T_{\mathrm{ph}}}$:

$$\rho_1 v_i = a_i v_i, \quad (65)$$

$$\rho_s u_j = b_j u_j, \quad (66)$$

$$\rho_c^{T_{\mathrm{ph}}} w_k = c_k w_k. \quad (67)$$

Here, $a_i, b_j \in [0,1]$, whereas c_k can be negative. The eigenvalues of the partially transposed full density matrix $\rho^{\Gamma}_{\mathrm{ph}\cup\mathrm{el}}$ are $\lambda_{i,j,k} = a_i b_j c_k$. Then the negativity reads as

$$\mathcal{N} = \sum_{\lambda_{i,j,k}<0}|\lambda_{i,j,k}| = \underbrace{\sum_i a_i}_{=1}\underbrace{\sum_j b_j}_{=1}\sum_{k \text{ with } c_k<0}|c_k| = \sum_{k \text{ with } c_k<0}|c_k|. \quad (68)$$

The sum of the magnitudes of the negative eigenvalues of the partially transposed full density matrix $\rho^{\Gamma}_{\mathrm{ph}\cup\mathrm{el}}$ equals the sum of the magnitudes of the negative eigenvalues of $\rho_c^{T_{\mathrm{ph}}}$. Hence we obtain the negativity by investigating only $\rho_c^{T_{\mathrm{ph}}}$. Since this is a Gaussian density matrix, we can determine the logarithmic entanglement negativity from its covariance matrix, which has dimension $4N \times 4N$ [40]. This method has been used to investigate the front dynamics of the harmonic chain [42] and later to analytically derive the dynamics after a sudden quench [50]. The elements of the covariance matrix are the real parts of all possible expectation values of coordinate and momentum products, for any arbitrary but fixed ordering of the operators. We order the rows and columns of the covariance matrix in such a way that it is block diagonal. It then takes the form

$$\begin{pmatrix} \mathrm{Re}\langle Q_{k,c}Q_{k,c}\rangle & \mathrm{Re}\langle Q_{k,c}q_{k,0,1}\rangle & 0 & 0 \\ \mathrm{Re}\langle Q_{k,c}q_{k,0,1}\rangle & \mathrm{Re}\langle q_{k,0,1}q_{k,0,1}\rangle & 0 & 0 \\ 0 & 0 & \mathrm{Re}\langle P_{k,c}P_{k,c}\rangle & \mathrm{Re}\langle P_{k,c}p_{k,0,1}\rangle \\ 0 & 0 & \mathrm{Re}\langle P_{k,c}p_{k,0,1}\rangle & \mathrm{Re}\langle p_{k,0,1}p_{k,0,1}\rangle \end{pmatrix} \quad (69)$$

for the cosine modes and

$$\begin{pmatrix} \mathrm{Re}\langle Q_{k,s}Q_{k,s}\rangle & \mathrm{Re}\langle Q_{k,s}q_{k,0,2}\rangle & 0 & 0 \\ \mathrm{Re}\langle Q_{k,s}q_{k,0,2}\rangle & \mathrm{Re}\langle q_{k,0,2}q_{k,0,2}\rangle & 0 & 0 \\ 0 & 0 & \mathrm{Re}\langle P_{k,s}P_{k,s}\rangle & \mathrm{Re}\langle P_{k,s}p_{k,0,2}\rangle \\ 0 & 0 & \mathrm{Re}\langle P_{k,s}p_{k,0,2}\rangle & \mathrm{Re}\langle p_{k,0,2}p_{k,0,2}\rangle \end{pmatrix} \quad (70)$$

for the sine modes. To get the covariance matrix of the partial transpose, we have to multiply every $P_{k,s}$ and $P_{k,c}$ by -1 in Eqs. (69) and (70). We then obtain the logarithmic negativity from the symplectic eigenvalues of the covariance matrix of the partial transpose [46],

$$\mathcal{E}_{\mathcal{N}} = -\sum_{\lambda}\ln\min(1,\lambda), \quad (71)$$

where the sum runs over all symplectic eigenvalues. For our case, we find

$$\mathcal{E}_{\mathcal{N}} = -4\sum_{k,\pm}\ln\min(1,\sqrt{\Lambda_{k,\pm}}), \quad (72)$$

where

$$\Lambda_{k,\pm} = \tfrac{1}{2}\left[a_k \pm \sqrt{a_k^2 + 4b_k - 4d_k}\right], \quad (73)$$

with

$$a_k = \langle Q_{k,s}Q_{k,s}\rangle\langle P_{k,s}P_{k,s}\rangle + \langle q_{k,0,2}q_{k,0,2}\rangle\langle p_{k,0,2}p_{k,0,2}\rangle + 2\langle P_{k,s}p_{k,0,2}\rangle\langle Q_{k,s}q_{k,0,2}\rangle, \quad (74)$$

$$b_k = (\langle Q_{k,s}q_{k,0,2}\rangle\langle P_{k,s}P_{k,s}\rangle - \langle q_{k,0,2}q_{k,0,2}\rangle\langle P_{k,s}p_{k,0,2}\rangle) \times (\langle Q_{k,s}q_{k,0,2}\rangle\langle p_{k,0,2}p_{k,0,2}\rangle - \langle P_{k,s}p_{k,0,2}\rangle\langle Q_{k,s}Q_{k,s}\rangle), \quad (75)$$

$$d_k = (\langle Q_{k,s}Q_{k,s}\rangle\langle P_{k,s}P_{k,s}\rangle - \langle P_{k,s}p_{k,0,2}\rangle\langle Q_{k,s}q_{k,0,2}\rangle) \times (\langle q_{k,0,2}q_{k,0,2}\rangle\langle p_{k,0,2}p_{k,0,2}\rangle - \langle P_{k,s}p_{k,0,2}\rangle\langle Q_{k,s}q_{k,0,2}\rangle). \quad (76)$$

In the general case, a positive value of the logarithmic negativity implies violation of separability, but a zero value does not imply separability. However, our model effectively

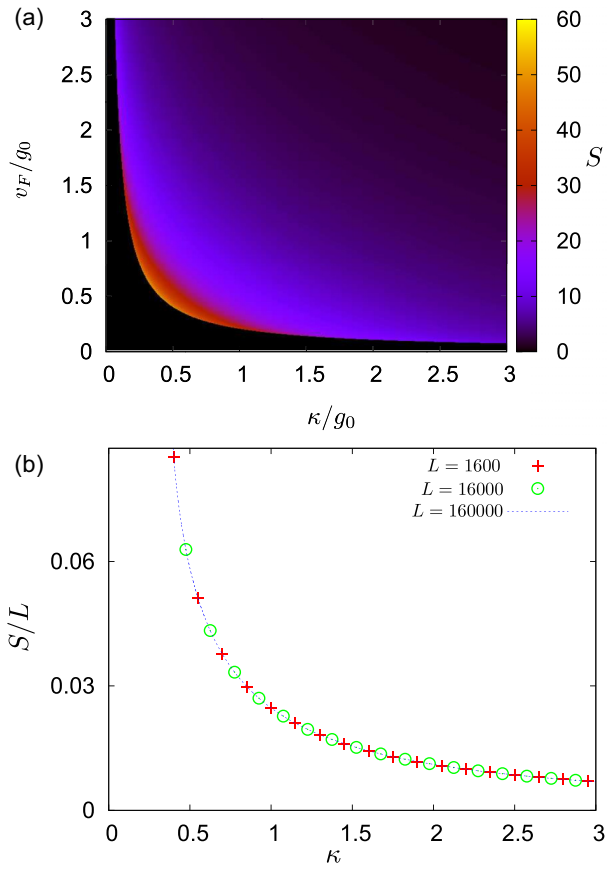

FIG. 1. Ground-state entanglement for the original noninteracting Wentzel-Bardeen model. (a) Entanglement entropy S between the lattice and the electrons for a chain of length $L = 200$, as a function of the lattice stiffness κ and the Fermi velocity v_f. In the black regions close to the axes, the system is unstable since $v_f < \pi g_0^2/16\kappa$. (b) Entanglement entropy per length as a function of the stiffness κ for $v_f = g_0/2$ for various system sizes.

consists of pairs of mutually coupled harmonic oscillators. It has been shown in Ref. [51] that in this case, zero logarithmic negativity is equivalent to separability.

Since Loss and Martin [39] and, recently, Dorn *et al.* [52] for topological-insulator nanowires have employed continuum descriptions of the phonons, the continuum limit of our lattice description is also of interest. This limit can be obtained in a straightforward manner, as shown in Appendix.

IV. RESULTS

In this section, we evaluate the expressions derived in Sec. III for two sets of parameters. The first set corresponds to the original Wentzel-Bardeen model without electron-electron interaction and with linear electron-phonon coupling, $g_k \sim k$, whereas the second describes a more realistic setting including electron-electron interaction and with the electron-phonon coupling scaling as $g_k \sim \sqrt{k}$.

A. Noninteracting model

In this section, we investigate the original form of the Wentzel-Bardeen model [24,25], with the electron-phonon

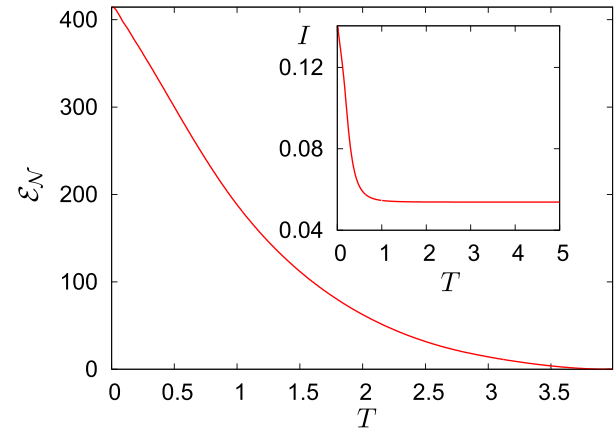

FIG. 2. Logarithmic negativity $\mathcal{E}_\mathcal{N}$ of the noninteracting Wentzel-Bardeen model as a function of temperature for $L = 100$, $\kappa = v_f = 1$, and $g_0 = 0.1$. Inset: Mutual information as a function of temperature for the same parameters.

coupling $g_k = g_0 k$. The stability criterion then becomes

$$2\omega_k^2 \Omega_k > g_k^2 \frac{k}{2\pi}, \tag{77}$$

which agrees with the results of Refs. [24,25]. If one would consider $g_k \sim \sqrt{k}$, which we do not do in this section, the noninteracting model would be unstable for *every* coupling strength since the left-hand side of Eq. (77) scales with $\sim k^3$ and the right-hand side would then scale with $\sim k^2$. We return to this point in the following section.

For a sine-shaped dispersion of the phonons, first the highest-energy $k = \pi$ mode becomes unstable, and the stable region is characterized by

$$v_f > \frac{\pi}{16} \frac{g_0^2}{\kappa}. \tag{78}$$

In the literature [24,25,30], there was a series of investigations to clarify the physical nature of this singularity. From our point of view, we use here a simple model without any anharmonic terms, which is only physical for a subset of the possible parameters. If the lattice is unstable in this model, the only consequence is that in the corresponding regime the anharmonic terms cannot be neglected.

The entanglement entropy at temperature $T = 0$ is shown as a function of the lattice stiffness and the Fermi velocity in Fig. 1. The entropy diverges close to the Wentzel-Bardeen singularity and is proportional to the system size, $S \propto L$.

The logarithmic entanglement negativity is plotted in Fig. 2. It decreases with increasing temperature and becomes exactly zero at and above a certain temperature. In this noninteracting case the transition temperature is independent of the system size. Similar behavior was observed in Ref. [40] for the logarithmic entanglement negativity of a bisectioned harmonic chain.

The mutual information is shown in the inset of Fig. 2. It decreases with increasing temperature and for high temperatures approaches a nonzero constant. This nonzero high-temperature value is a consequence of the infinite bandwidth of the model. In a model with a finite bandwidth, the

bandwidth sets a temperature scale, and one expects the mutual information to fall exponentially to zero above this scale.

B. Interacting Wentzel-Bardeen model

In this section, we consider a nonzero electron-electron interaction and electron-phonon coupling of the form $g_k = \tilde{g}_0\sqrt{k}$. As noted above, for the noninteracting model this type of coupling always causes an instability. We assume that the interaction between electrons moving in the same direction is not too strongly screened, i.e., that it shows a singularity of the form

$$h_k = \frac{h_0}{|k|^{1+\alpha}} \tag{79}$$

for small k, with sufficiently large α. The interaction between electrons moving in opposite directions is assumed to show the same functional relationship but shifted by the momentum transfer $2k_F$ between right-moving and left-moving electrons at the Fermi energy, i.e.,

$$f_k = \frac{f_0}{(|k| + 2k_F)^{1+\alpha}}. \tag{80}$$

Since f_k is nearly constant for low-energy modes, its specific form should not affect the qualitative results.

Under these assumptions, the left-hand side of the stability criterion, Eq. (28), is proportional to $k^{2+2\alpha}$, while the right-hand side is proportional to $k^{2+\alpha}$. We conclude that for $\alpha \geqslant 0$ the system can be stable. Detailed stability investigation can be performed by plotting the two sides of Eq. (28).

Results for the zero-temperature entanglement entropy of the interacting model are shown in Fig. 3(a). The entanglement increases with the electron-phonon coupling constant $\tilde{g}_0$ and decreases with the electron-electron interaction parameter h_0. Too large h_0 or too large $\tilde{g}_0$ render the system unstable. The entanglement entropy diverges when $\tilde{g}_0$ approaches the stability limit [see Fig. 3(b)] but remains finite if the stability limit is reached by increasing h_0.

It is also of interest to check how the entanglement entropy of a finite region scales with its size. It is known that the entanglement entropy of a coupled-oscillator system defined on a lattice follows an area law, i.e., the entanglement entropy between two subsystems scales with the size of the surface dividing the subsystems, which for a chain is a point, scaling with L^0. On the other hand, the entanglement entropy of a fermionic system generally follows an area law with log corrections [53,54]. We have calculated the entanglement entropy between a finite part of the lattice of length $l < L$ and the rest of the system, consisting of the rest of the lattice and all electronic degrees of freedom; see Fig. 3(c). We evidently find volume-law scaling, $S_l \sim l$. The entanglement entropy between the whole lattice and the electrons is proportional to the full system size, $S \sim L$. Similar behavior has been reported [55] for the intercomponent entanglement entropy of a two-component bosonic gas. We suggest that a similar phenomenon may also occur for trapped cold atoms in an optical resonator, where the photons play the role of the coupled bosons.

Results for the mutual information are shown in Fig. 4(a). The mutual information first decreases for increasing temperature, reaches a minimum, and then increases again, approaching a nonzero constant for high temperatures.

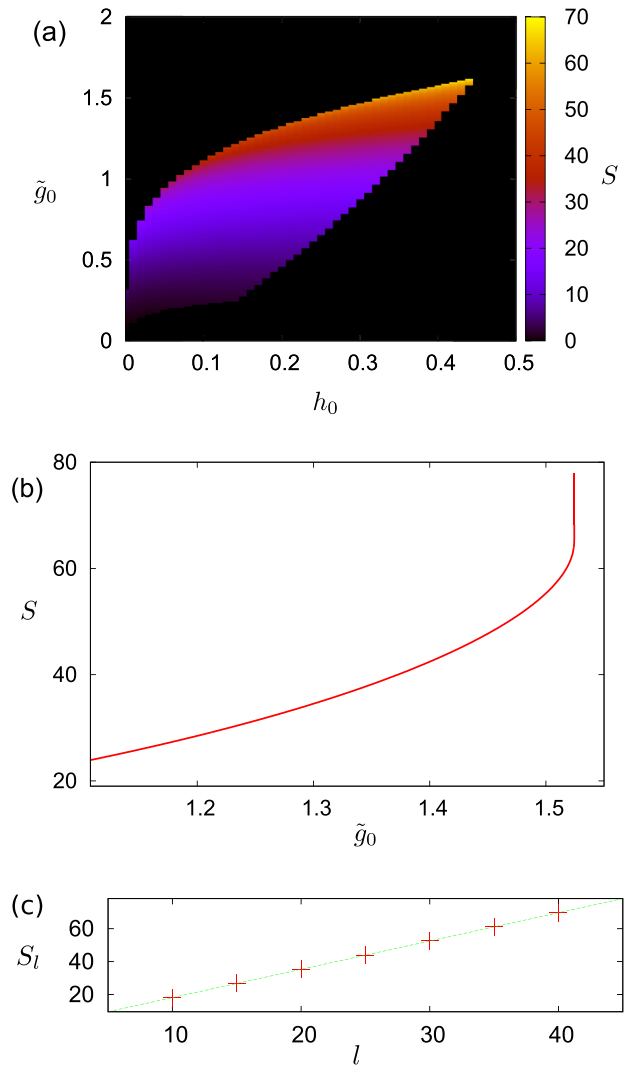

FIG. 3. (a) Entanglement entropy S for the interacting Wentzel-Bardeen model as a function of the electron-electron interaction parameter h_0 and the electron-phonon coupling parameter $\tilde{g}_0$. The Fermi velocity and the lattice stiffness are taken to be $v_f = \kappa = 1$. The black region denotes that the system is unstable. (b) Entanglement entropy as a function of $\tilde{g}_0$ for the same parameters as in (a) and $h_0 = 0.35$. (c) Entanglement entropy between a finite interval of the lattice of length $l < L$ and the rest of the system, including the other part of the lattice and all electronic degrees of freedom.

To address the range of validity of our description, we plot in the inset of Fig. 4(a) the von Neumann entropy of the reduced density matrix of the electrons. While our calculations are exact for the investigated model, the model is artificial in that the electronic bands are strictly linear over all momenta and energies. A real material is expected to show a linear spectrum close to the Fermi energy but deviations from linearity away from it. In this case, one can still describe the low-energy excitations within Luttinger-liquid theory, but results become unphysical beyond this regime. Let us consider a system with N_{tot} single-particle states, of which $N_{\text{lin}} < N_{\text{tot}}$

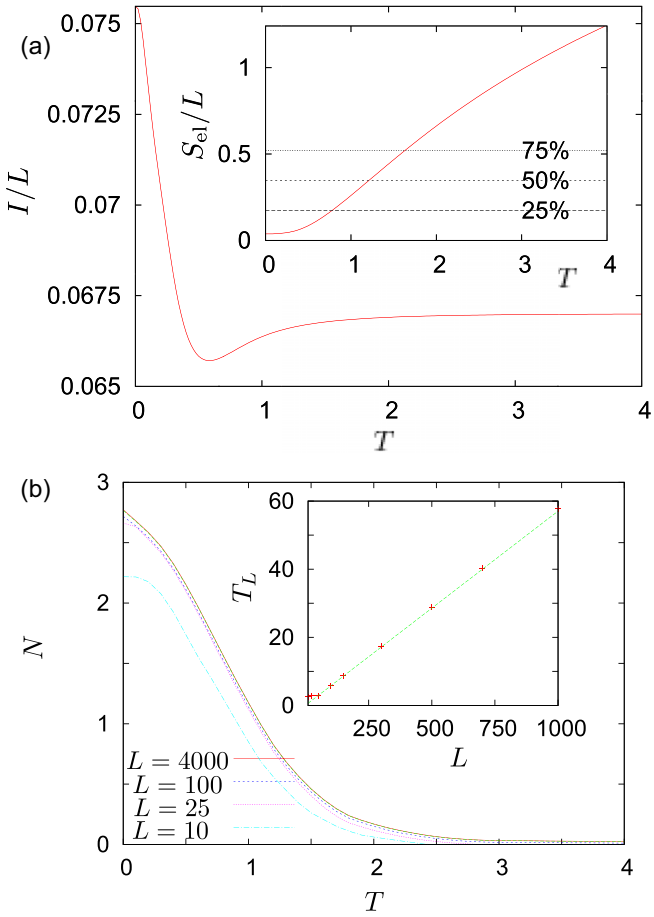

FIG. 4. (a) Mutual information I per length for the interacting system as a function of temperature for $L = 200$, $\kappa = v_f = 1$, and $\tilde{g}_0 = h_0 = f_0 = 1$. The inset shows the von Neumann entropy $S_{\rm el}$ of the reduced density matrix of the electrons; the horizontal lines denote the maximal possible entropies in a system with electron density $\rho_{\rm el} = 1$ and different lengths of the linear part of the spectrum, given in percent of the spectrum, as explained in the text. (b) Logarithmic negativity $\mathcal{E}_\mathcal{N}$ per length as a function of temperature for $\kappa = v_f = 1$, $\tilde{g}_0 = 0.1$, and various system sizes. The inset shows the finite-size dependence of the characteristic temperature T_L at which $\mathcal{E}_\mathcal{N}$ vanishes for $\alpha = 1.0$.

belong to the linear part of the spectrum. The maximal von Neumann entropy per length of the reduced density matrix of the states in the linear spectrum is

$$\frac{S^{\rm max}_{\rm Neumann}}{L} = \frac{S^{\rm max}_{\rm Neumann}}{N_{\rm tot}/\rho_{\rm el}} = \frac{\rho_{\rm el}}{N_{\rm tot}} \ln\left(\frac{N_{\rm lin}}{N_{\rm lin}/2}\right), \tag{81}$$

where $\rho_{\rm el}$ is the real-space electron concentration and the argument of the logarithm is a binomial coefficient. In the thermodynamic limit $N_{\rm lin} \gg 1$ and $N_{\rm tot} \gg 1$ with $N_{\rm lin}/N_{\rm tot} =$ const, one gets

$$\frac{S^{\rm max}_{\rm Neumann}}{L} \cong \ln(2)\, \rho_{\rm el} \frac{N_{\rm lin}}{N_{\rm tot}}. \tag{82}$$

Comparing the von Neumann entropy $S_{\rm el}$ of the electrons with this limit, one can check the validity of the Luttinger-liquid description. The limits are shown in the inset of Fig. 4(a). Comparing with the main panel, we conclude that the initial decrease in and the minimum of the mutual information are correctly described since in this regime $S_{\rm el}$ is still far below the entropic bound. The high-temperature plateau may also be reached, but in realistic systems with finite bandwidth this plateau is truncated when $S_{\rm el}$ reaches the bound.

Figure 4(b) shows the logarithmic entanglement negativity. The logarithmic negativity is extensive, $\mathcal{E}_\mathcal{N} \sim L$, for large L. It decreases with increasing temperature and in a finite system becomes exactly zero above a characteristic temperature T_L. The temperature T_L is connected to the smallest wave number $2\pi/L$ in the system. By expanding Eq. (73) for small k, using $h_k \gg \tilde{g}_0\sqrt{k} \gg v_F k$, we obtain a real number.

$$T_L = \frac{5}{4\pi(2\pi)^\alpha \ln 2}\, h_0\, L^\alpha. \tag{83}$$

Hence, for $\alpha = 0$ the characteristic temperature T_L is independent of the system length L. Note that $\alpha = 0$ is lying at the edge of the range of stability but the stability criterion, Eq. (28), can be satisfied for suitable system parameters. For less strongly screened interaction, i.e., $\alpha > 0$, the characteristic temperature grows with the system size and diverges in the thermodynamic limit. A similar sharp disappearance of the negativity has been reported in Refs. [40,56].

V. SUMMARY AND CONCLUSIONS

To summarize, we have addressed correlations and entanglement between the electronic (charge) and lattice degrees of freedom of a one-dimensional chain as a prototype for crystalline solids. We have calculated the entanglement entropy at zero temperature and the mutual information and logarithmic entanglement negativity at finite temperatures. This has been done for two models: on the one hand, the original Wentzel-Bardeen model without electron-electron interaction and with electron-phonon coupling linear in momentum and, on the other hand, a generalized Wentzel-Bardeen-Luttinger model with electron-electron interaction and electron-phonon coupling scaling as the square root of momentum. For the artificial model with infinite bandwidth, the entanglement entropy diverges for sufficiently strong electron-phonon coupling at the Wentzel-Bardeen singularity. The Luttinger description is expected to break down as this singularity is approached. We conjecture that in systems with finite bandwidth the entanglement entropy per length reaches a maximum instead of diverging. This is an interesting issue for future studies.

As noted above, the entanglement entropy of a coupled-oscillator system follows an area law, whereas the entanglement entropy of a fermionic system generally follows an area law with log corrections [53,54]. However, if we consider these systems in their most natural physical realizations, i.e., the phonon and electron subsystems of a solid, the situation changes. We have found that the entanglement entropy between a subset of the lattice of length $l < L$ and the rest of the system shows volume-law scaling, $S_l \sim l$, due to the interaction between the electron and lattice subsystems. Consequently, the entanglement entropy between the whole lattice and the electrons is proportional to the full length, $S \propto L$.

To check the validity of the Luttinger description for real systems with finite bandwidth, we have evaluated the

von Neumann entropy of the reduced density matrix of the electrons (at $T = 0$ this is the entanglement entropy). This electronic entropy must satisfy an upper bound, the violation of which signals the breakdown of our description. We find that at temperatures corresponding to thermal energies that are low compared with the electronic bandwidth, our description is valid.

Both the mutual information and the logarithmic negativity initially decrease with increasing temperature. The mutual information goes through a minimum and approaches a finite constant for $T \to \infty$. For sufficiently large electronic bandwidth, this plateau can still exist, but we conjecture that it is cut off at high temperatures when the electronic entropy starts to violate the aforementioned bound. The logarithmic negativity monotonously decreases with increasing temperature and becomes zero above a characteristic temperature, which implies that the entanglement disappears [51]. The characteristic temperature increases with system size if the electron-electron interaction is unscreened or weakly screened. However, for sufficiently strong screening, i.e., for an interaction of sufficiently short range, the characteristic temperature remains finite in the thermodynamic limit, indicating the presence of a real phase transition with the logarithmic entanglement negativity acting as its order parameter. This result is quite different from the finite-temperature transition found earlier for a bisectioned harmonic chain [40]. In our case, the electronic and lattice subsystems are coupled over the full length of the chain and nevertheless lose all entanglement at a characteristic temperature.

The entanglement entropy can be used as a self-consistency tool to check whether we have a sufficiently large bandwidth in a real system for a Luttinger description; see Eq. (82). This check would be especially useful when interesting physics emerges close to the Wentzel-Bardeen instability. For example, in Ref. [52], a topological-insulator nanowire is investigated, and the authors set up an effective model where one electron band is coupled to the lattice modes described by a continuum theory. They find an interesting transition between a normal-metal-like region and a superconductor-like region in the vicinity of the Wentzel-Bardeen instability.

A further point is that the entanglement entropy seems to be analytical in the whole region of stability, which may be surprising since coupled Luttinger-liquid–phonon systems are known to have nontrivial "phase diagrams" [39,52]. The origin of this analytical behavior is that the transitions displayed in these phase diagrams are not true quantum phase transitions but rather signal the strongest (most slowly decreasing) correlation function. Usually, all correlation functions decay with a power law. In non-Luttinger systems with finite bandwidth coupled to phonons, true quantum phase transitions do exist. An interesting question for future research is what the electron-phonon entanglement entropy looks like in the proximity of these transitions.

ACKNOWLEDGMENTS

The authors thank Zoltán Zimborás, Szilárd Szalay, and Vrana Péter for stimulating discussions. The authors acknowledge financial support from the Deutsche Forschungsgemeinschaft through Collaborative Research Center SFB 1143, project A04, and the Cluster of Excellence on Complexity and Topology in Quantum Matter ct.qmat (EXC 2147). G.R. acknowledges financial support from the National Research, Development and Innovation Office NKFIH, Hungary, under Grants No. K135220 and No. K128989. This research was supported by the Ministry of Innovation and Technology and the National Research, Development and Innovation Office within the Quantum Information National Laboratory of Hungary.

APPENDIX: CONTINUUM LIMIT

Although the mass distribution of a real lattice is discrete, a continuum description has been used successfully to describe the low-energy sector of carbon nanotubes and topological-insulator nanowires [27,28,30,52]. In the main text, we have started from the physically more natural discrete description of the lattice. In this Appendix, we consider the continuum limit of $N \to \infty$ and $a_0 \to 0$ with constant L, constant mass density ρ, and constant strain. We define

$$\check{\kappa} \equiv a_0 \kappa = \text{const}, \tag{A1}$$

$$\check{\rho} \equiv \frac{m}{a_0} = \text{const} \tag{A2}$$

and replace

$$\frac{g(|la_0 - x|)}{a_0} \to \check{g}(|x - y|), \tag{A3}$$

$$a_0 \sum_{l=1}^{N} \to \int_0^L dy. \tag{A4}$$

The fields describing the lattice in the continuum limit are $\phi(x) = \lim_{N\to\infty} q_{[x/a_0]}$ and $\pi(x) = \lim_{N\to\infty} p_{[x/a_0]}$. We introduce a cutoff wave number k_{cut} in the electron-phonon coupling. This cutoff is physically necessary since the continuum limit introduces low wavelengths, which are simply not there in real physical systems. Starting from the discrete description, the wave number is automatically cut off by the finite Brillouin zone.

In the continuum limit for the phonons (the electrons are described by continuum fields in any case), the Hamiltonian becomes

$$\begin{aligned} H = & -\sum_{\sigma=\pm 1/2} \int_0^L \frac{dx}{2\pi}\, v_f [\, {}^{*}_{*}\Psi^{\dagger}_{\sigma,L}(x)\, i\partial_x \Psi_{\sigma,L}(x)\, {}^{*}_{*} \\ & + {}^{*}_{*}\Psi^{\dagger}_{\sigma,R}(x)\, i\partial_x \Psi_{\sigma,R}(x)\, {}^{*}_{*}] \\ & + \int_0^L dx \frac{1}{2\check{\rho}}\, \pi^2 + \frac{\check{\kappa}}{2}\, (\partial_x \phi)^2 \\ & + \frac{1}{\sqrt{L}} \int_0^L dx\, \phi(x) \int_0^L dy\, [\hat{n}_L(y) + \hat{n}_R(y)]\, \check{g}(|y - x|_L) \\ & + \frac{4}{L} \int_0^L dx \int_0^L dy\, (\hat{n}_L(x), \hat{n}_R(y)) \\ & \times \begin{pmatrix} h(x-y) & \frac{1}{2} f(x-y) \\ \frac{1}{2} f(x-y) & h(x-y) \end{pmatrix} \begin{pmatrix} \hat{n}_L(x) \\ \hat{n}_R(y) \end{pmatrix}. \end{aligned} \tag{A5}$$

Furthermore, our equation for the entanglement entropy becomes

$$S = \frac{L}{2\pi}\int_0^{k_{\rm cut}} dk\big[s(\langle Q_{S,k}^2\rangle\langle P_{S,k}^2\rangle) + s(\langle Q_{C,k}^2\rangle\langle P_{C,k}^2\rangle)\big]. \quad \text{(A6)}$$

Note that the only difference compared with the previous equation (48) is the cutoff wave number in the integration limit. The entanglement entropy can also be expressed using the variables of the fermionic subsystem,

$$S = \frac{L}{2\pi}\int_0^{\infty} dk\big[s(\langle q_{k,0,1}^2\rangle\langle p_{k,0,1}^2\rangle) + s(\langle q_{k,0,2}^2\rangle\langle p_{k,0,2}^2\rangle)\big]. \quad \text{(A7)}$$

This equation may be useful if one prefers integrating out the phonons and working only with the fermionic variables. We note that the two Eqs. (A6) and (A7) give equal results at zero temperature, where the entropy of the reduced density matrix is the entanglement entropy, and give different results at finite temperatures, as discussed in Ref. [57]. The mutual information is given by Eq. (59), which we repeat for convenience:

$$I = S(\mathrm{Tr}_{\rm ph}\rho_c) + S(\mathrm{Tr}_{\rm el}\rho_c) - S(\rho_c). \quad \text{(A8)}$$

In the continuum limit, the three terms are given by

$$S(\mathrm{Tr}_{\rm ph}\rho_c) = \frac{L}{2\pi}\int_0^{\infty} dk\big[s(\langle Q_{S,k}^2\rangle\langle P_{S,k}^2\rangle) + s(\langle Q_{C,k}^2\rangle\langle P_{C,k}^2\rangle)\big], \quad \text{(A9)}$$

$$S(\mathrm{Tr}_{\rm el}\rho_c) = \frac{L}{2\pi}\int_0^{\infty} dk\big[s(\langle q_{k,0,1}^2\rangle\langle p_{k,0,1}^2\rangle) + s(\langle q_{k,0,2}^2\rangle\langle p_{k,0,2}^2\rangle)\big], \quad \text{(A10)}$$

$$S(\rho_c) = 2\frac{L}{2\pi}\int_0^{\infty} dk\Big[\frac{\sqrt{\lambda}_{k,\pm}}{\exp(\beta\sqrt{\lambda}_{k,\pm})-1} - \ln(1-\exp(-\beta\sqrt{\lambda}_{k,\pm}))\Big]. \quad \text{(A11)}$$

When one takes the difference in Eq. (A8), the parts between $k_{\rm cut}$ and ∞ in the integrals cancel each other.

To summarize, we find that the formulas derived for the discrete harmonic lattice can be generalized to the continuum limit in a straightforward way.

[1] E. Maxwell, Isotope effect in the superconductivity of mercury, Phys. Rev. **78**, 477 (1950).

[2] C. A. Reynolds, B. Serin, W. H. Wright, and L. B. Nesbitt, Superconductivity of isotopes of mercury, Phys. Rev. **78**, 487 (1950).

[3] W. D. Allen, R. H. Dawton, M. Bär, K. Mendelson, and J. L. Olsen, Superconductivity of tin isotopes, Nature (London) **166**, 1071 (1950).

[4] L. N. Cooper, Bound electron pairs in a degenerate Fermi gas, Phys. Rev. **104**, 1189 (1956).

[5] J. Bardeen, L. N. Cooper, and J. R. Schrieffer, Microscopic theory of superconductivity, Phys. Rev. **106**, 162 (1957).

[6] J. Bardeen, L. N. Cooper, and J. R. Schrieffer, Theory of superconductivity, Phys. Rev. **108**, 1175 (1957).

[7] R. E. Peierls, *Quantum Theory of Solids* (Oxford University Press, Oxford, 1955), p. 108.

[8] P. A. Lee, T. M. Rice, and P. W. Anderson, Fluctuation Effects at a Peierls Transition, Phys. Rev. Lett. **31**, 462 (1973).

[9] B. Braunecker, G. I. Japaridze, J. Klinovaja, and D. Loss, Spin-selective Peierls transition in interacting one-dimensional conductors with spin-orbit interaction, Phys. Rev. B **82**, 045127 (2010).

[10] G. Grüner, The dynamics of charge density waves, Rev. Mod. Phys. **60**, 1129 (1988).

[11] A. Ványolos, B. Dóra, and A. Virosztek, Unconventional charge-density waves driven by electron-phonon coupling, Phys. Rev. B **73**, 165127 (2006).

[12] J. H. Miller, C. Ordóñez, and E. Prodan, Time-Correlated Soliton Tunneling in Charge and Spin Density Waves, Phys. Rev. Lett. **84**, 1555 (2000).

[13] A. B. Midgal, Interaction between electrons and lattice vibrations in a normal metal, Sov. Phys. JETP **7**, 996 (1958).

[14] G. M. Éliashberg, Interactions between electrons and lattice vibrations in a superconductor, Sov. Phys. JETP **11**, 696 (1960).

[15] A. S. Mishchenko, N. Nagaosa, and N. Prokof'ev, Diagrammatic Monte Carlo Method for Many-Polaron Problems, Phys. Rev. Lett. **113**, 166402 (2014).

[16] A. Mishchenko, N. Prokof'ev, A. Sakamoto, and B. Svistunov, Diagrammatic quantum Monte Carlo study of the Fröhlich polaron, Phys. Rev. B **62**, 6317 (2000).

[17] N. V. Prokof'ev and B. V. Svistunov, Polaron Problem by Diagrammatic Quantum Monte Carlo, Phys. Rev. Lett. **81**, 2514 (1998).

[18] J. del Pino, F. A. Y. N. Schröder, A. W. Chin, J. Feist, and F. J. Garcia-Vidal, Tensor Network Simulation of Non-Markovian Dynamics in Organic Polaritons, Phys. Rev. Lett. **121**, 227401 (2018).

[19] L. Amico, R. Fazio, A. Osterloh, and V. Vedral, Entanglement in many-body systems, Rev. Mod. Phys. **80**, 517 (2008).

[20] Sz. Szalay, G. Barcza, T. Szilvási, L. Veis, and Ö. Legeza, The correlation theory of the chemical bond, Sci. Rep. **7**, 2237 (2017).

[21] D. A. Abanin, E. Altman, I. Bloch, and M. Serbyn, Colloquium: Many-body localization, thermalization, and entanglement, Rev. Mod. Phys. **91**, 021001 (2019).

[22] Y. Shi, L. Duan, and G. Vidal, Classical simulation of quantum many-body systems with a tree tensor network, Phys. Rev. A **74**, 022320 (2006).

[23] J. L. Sanz-Vicario, J. F. Pérez-Torres, and G. Moreno-Polo, Electronic-nuclear entanglement in H_2^+: Schmidt decomposition of non-Born-Oppenheimer wave functions expanded in nonorthogonal basis sets, Phys. Rev. A **96**, 022503 (2017).

[24] G. Wentzel, The interaction of lattice vibrations with electrons in a metal, Phys. Rev. **83**, 168 (1950).

[25] J. Bardeen, Electron-vibration interactions and superconductivity, Rev. Mod. Phys. **23**, 261 (1951).

[26] S. Engelsberg and B. B. Varga, One-dimensional electron-phonon model, Phys. Rev. **136**, A1582 (1964).

[27] R. Egger and A. O. Gogolin, Effective Low-Energy Theory for Correlated Carbon Nanotubes, Phys. Rev. Lett. **79**, 5082 (1997).
[28] C. Kane, L. Balents, and M. P. A. Fisher, Coulomb Interactions and Mesoscopic Effects in Carbon Nanotubes, Phys. Rev. Lett. **79**, 5086 (1997).
[29] H. Suzuura and T. Ando, Phonons and electron-phonon scattering in carbon nanotubes, Phys. Rev. B **65**, 235412 (2002).
[30] A. De Martino and R. Egger, Acoustic phonon exchange, attractive interactions, and the Wentzel-Bardeen singularity in single-wall nanotubes, Phys. Rev. B **67**, 235418 (2003).
[31] R. Rosati, F. Dolcini, and F. Rossi, Electron-phonon coupling in metallic carbon nanotubes: Dispersionless electron propagation despite dissipation, Phys. Rev. B **92**, 235423 (2015).
[32] A. Benyamini, A. Hamo, S. V. Kusminskiy, F. von Oppen, and S. Ilani, Real-space tailoring of the electron–phonon coupling in ultraclean nanotube mechanical resonators, Nat. Phys. **10**, 151 (2014).
[33] C. H. Bennett, H. J. Bernstein, S. Popescu, and B. Schumacher, Concentrating partial entanglement by local operations, Phys. Rev. A **53**, 2046 (1996).
[34] J. Eisert, M. Cramer, and M. B. Plenio, Colloquium: Area laws for the entanglement entropy, Rev. Mod. Phys. **82**, 277 (2010).
[35] V. Vedral, The role of relative entropy in quantum information theory, Rev. Mod. Phys. **74**, 197 (2002).
[36] A. Sanpera, R. Tarrach, and G. Vidal, Quantum separability, time reversal and canonical decompositions, arXiv:quant-ph/9707041.
[37] A. Sanpera, R. Tarrach, and G. Vidal, Local description of quantum inseparability, Phys. Rev. A **58**, 826 (1998).
[38] G. Vidal and R. F. Werner, A computable measure of entanglement, Phys. Rev. A **65**, 032314 (2002).
[39] D. Loss and T. Martin, Wentzel-Bardeen singularity and phase diagram for interacting electrons coupled to acoustic phonons in one dimension, Phys. Rev. B **50**, 12160 (1994).
[40] K. Audenaert, J. Eisert, M. B. Plenio, and R. F. Werner, Entanglement properties of the harmonic chain, Phys. Rev. A **66**, 042327 (2002).
[41] A. Coser, E. Tonni, and P. Calabrese, Entanglement negativity after a global quantum quench, J. Stat. Mech. (2014) P12017.
[42] V. Eisler and Z. Zimborás, Entanglement negativity in the harmonic chain out of equilibrium, New J. Phys. **16**, 123020 (2014).
[43] J. von Delft and H. Schoeller, Bosonization for beginners – refermionization for experts, Ann. Phys. (Berlin) **7**, 225 (1998).
[44] F. Bloch, Über die Quantenmechanik der Elektronen in Kristallgittern, Z. Phys. **52**, 555 (1929).
[45] F. Giustino, Electron-phonon interactions from first principles, Rev. Mod. Phys. **89**, 015003 (2017).
[46] I. Peschel, Entanglement in solvable many-particle models, Braz. J. Phys. **42**, 267 (2012).
[47] B. Dóra, I. Lovas, and F. Pollmann, Distilling momentum-space entanglement in Luttinger liquids at finite temperature, Phys. Rev. B **96**, 085109 (2017).
[48] S. Furukawa and Y. B. Kim, Entanglement entropy between two coupled Tomonaga-Luttinger liquids, Phys. Rev. B **83**, 085112 (2011).
[49] R. Lundgren, Y. Fuji, S. Furukawa, and M. Oshikawa, Entanglement spectra between coupled Tomonaga-Luttinger liquids: Applications to ladder systems and topological phases, Phys. Rev. B **88**, 245137 (2013).
[50] V. Alba and P. Calabrese, Quantum information dynamics in multipartite integrable systems, Europhys. Lett. **126**, 60001 (2019).
[51] R. F. Werner and M. M. Wolf, Bound Entangled Gaussian States, Phys. Rev. Lett. **86**, 3658 (2001).
[52] K. Dorn, A. De Martino, and R. Egger, Phase diagram and phonon-induced backscattering in topological insulator nanowires, Phys. Rev. B **101**, 045402 (2020).
[53] D. Gioev and I. Klich, Entanglement Entropy of Fermions in Any Dimension and the Widom Conjecture, Phys. Rev. Lett. **96**, 100503 (2006).
[54] S. Farkas and Z. Zimborás, The von Neumann entropy asymptotics in multidimensional fermionic systems, J. Math. Phys. (Melville, NY) **48**, 102110 (2007).
[55] T. Yoshino, S. Furukawa, and M. Ueda, Intercomponent entanglement entropy and spectrum in binary Bose-Einstein condensates, Phys. Rev. A **103**, 043321 (2021).
[56] S. Wald, R. Arias, and V. Alba, Entanglement and classical fluctuations at finite-temperature critical points, J. Stat. Mech. (2020) 033105.
[57] M. B. Plenio and S. Virmani, An introduction to entanglement measures, Quantum Inf. Comput. **7**, 1 (2007).